



---

## Investigating the Photocatalytic Activity of $\text{TiO}_2@ \text{WO}_3/\text{ZnO}$ Catalyst in the Waste Water Treatment Containing Alkanolamine Contaminants

Paymaneh Taghizadeh-Lendeh<sup>1</sup>, Amir Hossein Mohsen Sarrafi<sup>1</sup>, Afshar Alihosseini<sup>2,\*</sup>, Naeimeh Bahri-Laleh<sup>3</sup>

<sup>1</sup>Department of Chemistry, Central Tehran Branch, Islamic Azad University, P.O. Box. 1496969191, Tehran, Iran

<sup>2</sup>Department of Chemical Engineering, Central Tehran Branch, Islamic Azad University, P.O. Box.1496969191, Tehran, Iran

\*Corresponding Author Email: [Afs.alihosseini@iauctb.ac.ir](mailto:Afs.alihosseini@iauctb.ac.ir)

<sup>3</sup>Polymerization Engineering Department, Iran Polymer and Petrochemical Institute (IPPI), P.O. Box 14965/115, Tehran, Iran.

*Received: 06.12.2021*

*Accepted: 17.02.2022*

*Published: 18.02.2022*

---

### ABSTRACT

Natural gas has wide range of acid gas concentrations such as  $\text{CO}_2$  and  $\text{H}_2\text{S}$ . Alkanolamines dissolved in aqueous solutions are commonly employed to scrub  $\text{CO}_2$  and  $\text{H}_2\text{S}$  from natural gas. As a result, the high level of this pollutant is emitted through the waste water during cleaning. In this study a novel photocatalyst,  $\text{TiO}_2@ \text{WO}_3/\text{ZnO}$ , has been designed and fabricated. To prepare the catalyst with the highest performance, the optimized weight fraction of  $\text{WO}_3+\text{ZnO}$  (with 1:4 weight ratio) has been alloyed with  $\text{TiO}_2$ . The results from BET and BJH indicated that the synthesized catalyst had relatively high specific surface area ( $10.3 \text{ m}^2 \text{ g}^{-1}$ ) and meso-

---

pore structure with cavities diameter of 10.9 nm. The as-synthesized photocatalyst has been employed in the alkanolamine contaminant degradation of wastewater obtained from an industrial gas refinery plant in the presence of LED light. In this regard, the degradation of alkanolamine during time was monitored using UV-Vis and fluorescence spectroscopies. The obtained results confirmed high performance of the designed catalyst in the rapid treatment of the wastewater of gas refinery effluent at very low catalyst loading of only 0.5 wt.%, thereby making it a good candidate for the catalytic purposes. Finally, a possible mechanism for catalytic degradation of alkanolamine over  $\text{TiO}_2@/\text{WO}_3/\text{ZnO}$  was suggested.

**Keywords:** synthesis; degradation; gas refinery effluent;  $\text{TiO}_2@/\text{WO}_3/\text{ZnO}$  photocatalyst; alkanolamine.

## Introduction

Natural gas is one of the major energy resources in the world and its production is exceeding. It has a wide range of acid gas concentrations such as  $\text{CO}_2$  and  $\text{H}_2\text{S}$ . Due to the corrosiveness of these pollutants in the presence of water, the toxicity of  $\text{H}_2\text{S}$  and the ineffectiveness of  $\text{CO}_2$  in heating process, natural gas needs to be sweetened [1]. Alkanolamines dissolved in aqueous solutions are commonly employed to scrub  $\text{CO}_2$  from natural gas. As a result of aforementioned mechanism, the high level of this pollutant is emitted through the waste water during cleaning, maintenance and even shutdown of the absorption and desorption columns. This pollutant is toxic and dangerous to the environment and the polluted wastewater cannot be refined in the typical wastewater refineries [2, 3]. In fact, the release of alkanolamines in the industrial waste water from gas refinery effluents has raised many concerns and motivated many researchers to find the proper solutions for the efficient removal of these hazardous pollutants [4]. In this regard, many approaches such as the use of adsorbents, photodegradation, oxidative and membrane processes have been suggested [5-8]. Briefly, extensive research has been conducted on Photocatalysis: Fundamental Processes and Applications [9]: in the fields of Electronic structure: From basic principles to photocatalysis [10], Photodegradation processes [11], Using dyes to evaluate the photocatalytic activity [12], Advanced oxidation [13], The kinetic models in electron transfer processes [14], Fundamental developments in the zeolite process [15], Design of active

photocatalysts and visible light photocatalysis [16], New materials and equipment for photocatalytic degradation processes [17], Photocatalytic treatment of pollutants in aqueous media [18], and Photocatalytic reduction of CO<sub>2</sub> in hydrocarbon: A greener approach for energy production [19]. Among the proposed approaches, photocatalysis is extensively employed for the waste water treatment from gas refinery effluents. It is a catalytic degradation process mostly promoted by metallic catalysts such as Ti, W and Zn in an oxidizing environment [20, 21]. Owing to the significance of photocatalysis, extensive research has been conducted on this issue. Photocatalysis process in the presence of light to activate a substance and accordingly, the photocatalysts without any permanent chemical alteration happening to them, enhanced the chemical reactions velocity. These reactions can occur using homogeneous or heterogeneous photocatalysts. The later has been extensively attracted attentions because of its potential use in various fields from environmental applications to energy demand [22]. In this line, WO<sub>3</sub> semiconductor with an energy band gap of 2.7 eV has been deliberated as an effective nanoparticle together with some photocatalysts due to its excellent physiochemical stability and strong visible light response [23, 24]. To form heterojunction, WO<sub>3</sub> with ZnO nanoparticles might be an effective strategy to improve the photocatalytic performance. Indeed, WO<sub>3</sub> deposition improved the performance of WO<sub>3</sub>/ZnO photocatalyst by elimination of defects in the ZnO particles surface [25]. This composite has also been used to reduce and oxidize gases in the sensor and the treatment of gaseous phase pollutants [26, 27]. Although TiO<sub>2</sub> nanocomposites have wide applications in the Survival Viability of Cervical Cancer Cells [28] and brilliant blue dye degradation using visible light [29], particular attention has been placed on sedimentation techniques for photocatalytic decomposition in wastewater treatment applications. Furthermore, TiO<sub>2</sub> nanoparticles in combination with WO<sub>3</sub>/ZnO nanocomposite (i.e. TiO<sub>2</sub>@WO<sub>3</sub>/ZnO photocatalyst) has been practiced to progress the photocatalytic activity [30]. It seems that the concentration of tungsten and zinc oxide as well as TiO<sub>2</sub> can influence the catalytic performance of the final photocatalyst. Chemical oxygen demand (COD) often is used as a measurement of pollutants in wastewater. Other related analytical values are biochemical oxygen demand (BOD). In many cases, it is possible to correlate two or more of these values for a given sample. BOD is a measure of oxygen consumed by microorganisms under specific conditions. Some samples with very low COD or with highly heterogeneous solids content may need to be analyzed.

Results are further enhanced by reacting a maximum quantity of bichromate, provided that some residual bichromate remains. BOD testing is used to determine the relative oxygen requirements of wastewaters, polluted waters and effluents; its widest application is in measuring waste loadings to treatment plants and in evaluating the plants' BOD removal efficiency [31]. Degradation of alkanolamine as: Methyldiethanolamine (MDEA) pollutants of waste water of gas refinery by photocatalyst has not been studied and in this study, by reason of the environmental concern of polluted waste water, obtained from gas refinery effluents, and in the pursuit of our research on the design of novel heterogeneous catalysts [32-34], here we report the synthesis of an heterogeneous photocatalyst employed in the removal of toxic alkanolamine pollutants. In this regard, we focused more on the W:Zn:Ti ratio by changing weight fraction of the related ingredients to acquire efficient  $\text{TiO}_2@/\text{WO}_3/\text{ZnO}$  photocatalyst suitable in the degradation of alkanolamine pollutants of waste water.

## Experimental

### Materials

In this study sodium tungsten ( $\text{Na}_2\text{O}_4\text{W}$ ), titanium tetrachloride ( $\text{TiCl}_4$ ), zinc sulfate ( $\text{ZnSO}_4 \cdot 7\text{H}_2\text{O}$ ), ammonia ( $\text{NH}_3$ ), hydrochloric acid ( $\text{HCl}$ ), ammonium carbonate ( $(\text{NH}_4)_2\text{CO}_3$ ) and polyethylene glycol ( $\text{C}_{2n}\text{H}_{4n+2}\text{O}_{n+1}$ , with  $M_w=1000$  g/mol) were used for the synthesis of  $\text{TiO}_2@/\text{WO}_3/\text{ZnO}$  photocatalyst. Mercury(II) sulfate ( $\text{HgSO}_4$ ), potassium bichromate ( $\text{K}_2\text{Cr}_2\text{O}_7$ ), silver sulfate ( $\text{Ag}_2\text{SO}_4$ ), ferrous sulfate ( $\text{Fe}(\text{SO}_4)_2 \cdot 6\text{H}_2\text{O}$ ), manganese(II) sulfate ( $\text{MnSO}_4$ ), iodine (I), sodium thiosulfate ( $\text{Na}_2\text{S}_2\text{O}_3$ ) and starch ( $n(\text{C}_6\text{H}_{10}\text{O}_5)$ ), were used for the COD and BOD measurements. All the aforesaid chemicals and solvents, were of analytical grade, provided from Sigma-Aldrich, and used without any further purification. Distilled water was used in all the experiments.

### Synthesis of $\text{TiO}_2$ nanoparticles

For the synthesis of  $\text{TiO}_2$  nanoparticles a two necked round bottom flask was placed in an ice bath to supply the temperature of  $0^\circ\text{C}$ . 10 mL of  $\text{TiCl}_4$  was homogeneously dispersed in 20 mL deionized water and then, 20 mL of 25% ammonia was introduced to the aforementioned

solution in dropwise manner. The agitation was lasted for 1 h at 0 °C until the color changed to white color. Subsequently, the obtained TiO<sub>2</sub> nanoparticles were separated using a centrifuge, washed with distilled water repeatedly and dried in an oven at 100 °C for 3 hours.

### **Synthesis of WO<sub>3</sub> nanoparticles**

To this end, 2.5 g sodium tungstate was homogeneously dispersed in 25 mL deionized water. Appropriate amount of HCl (with the concentration of 3 M) was added dropwise into the aforementioned solution to reach pH = 1. The mixing process was lasted for 1 h till a yellow color solution was achieved. The prepared WO<sub>3</sub> particles were separated using a centrifuge, dried at 100 °C for 3 h and, subsequently, calcined at 500 °C for 1 h.

### **Synthesis of ZnO nanoparticles**

5 g of zinc sulfate was dissolved in 50 mL of deionized water and stirred until a completely homogeneous solution was achieved. Ammonia was gently dropped to the prepared solution till a white (milky) solution was achieved. The synthesized ZnO nanoparticles were separated using a centrifuge, washed several times with distilled water, dried in an oven at 100 °C for 3 h and, subsequently, calcined at 500 °C for 1 h.

### **Synthesis of WO<sub>3</sub> /ZnO photocatalyst**

WO<sub>3</sub>/ZnO photocatalyst was prepared according to the previously reported procedure [28, 35-37]. To this end, appropriate amount of hydrochloric acid (3 M) was added dropwise into a solution containing 1 g tungstate sulfate and 10 mL distilled water, to reach pH = 1. Afterward, a white (milky) solution containing 0.25 g of zinc sulfate, 10 mL distilled water and appropriate amount of ammonia was introduced into the aforementioned solution dropwise. Then, 0.3 g of ammonium carbonate in 10 mL of distilled water was also introduced into the reactor. The stirring was continued for 1 h, after which the formed WO<sub>3</sub>/ZnO particles were separated using a centrifuge, washed repeatedly with distilled water, dried in an oven at 100 °C for 3 h and, subsequently, calcined at 600 °C for 1 h.

### Optimization of WO<sub>3</sub>/ZnO photocatalyst

To reach a photocatalyst with an optimized weight percentage of W to Zn, five catalysts with different WO<sub>3</sub>/ZnO mass ratios (2:1, 1:1, 1:2, 1:4 and 1:6) were prepared. The absorption property of the synthesized photocatalysts was recorded by UV-Vis spectroscopy. In the achieved spectra, the WO<sub>3</sub>/ZnO photocatalyst with 4:1 mass ratio that demonstrated related  $\lambda_{\max}$  at higher wavelength, was selected as the best catalyst among the series [38, 39].

### Synthesis of TiO<sub>2</sub>@WO<sub>3</sub>/ZnO photocatalyst

A mixture containing 1:3 weight ratio of TiO<sub>2</sub> to WO<sub>3</sub>/ZnO (in 1:4 mass ratio of WO<sub>3</sub> to ZnO) was suspended in 30 mL of deionized water. 0.11 g of polyethylene glycol was homogeneously dispersed in 22 mL of deionized water and added dropwise to the aforementioned solution. After 2 h stirring, the synthesized TiO<sub>2</sub>@WO<sub>3</sub>/ZnO photocatalyst was separated using a centrifuge, dried in an oven at 100 °C for 3 h and, subsequently, calcined at 600 °C for 1 h.

### Optimization of TiO<sub>2</sub>@WO<sub>3</sub>/ZnO photocatalyst

To reach a photocatalyst with an optimized weight percentage of Ti to W and Zn, four catalysts with different TiO<sub>2</sub>@WO<sub>3</sub>/ZnO mass ratios (3:1, 10:1, 1:10, and 1:3) were synthesized. The as-prepared photocatalyst with 1:3 mass ratio in which the  $\lambda_{\max}$  had the highest value, was selected as the optimized photocatalyst among the studied samples.

### Checking seed effectiveness and analytical technique by using procedures in 5220B to make COD measurements

In the first stage, a composition comprising 0.4 mg of HgSO<sub>4</sub>, 10 mL of K<sub>2</sub>Cr<sub>2</sub>O<sub>7</sub>, 30 mL of H<sub>2</sub>SO<sub>4</sub> and Ag<sub>2</sub>SO<sub>4</sub> solution. 2 ml of unknown sample to volume up to 20 ml with distilled water so as not to cause it to turn green. They were added to a jouge balloon. Four boiling stones were thrown into a volumetric balloon and 30 mL of H<sub>2</sub>SO<sub>4</sub> and Ag<sub>2</sub>SO<sub>4</sub> solution was added to the solution. This step was slowly done with shaking and under a cold tap. The solution was placed on a Soxhlet oven and note the time after boiling. After 2 h, the solution was cooled and 3 drops of Freon Detector was added to it and the titration was continued with Fe(SO<sub>4</sub>)<sub>2</sub>.6H<sub>2</sub>O solution

until its color changed from orange to light brown. The above steps were simultaneously performed for the control (instead of the distilled water sample). Using the following formula, the amount of COD in the samples was obtained.

$$\text{COD ((mg/L) O}_2) = \frac{(A-B) \times 8000 \times N}{C}$$

Where, A was control ferrosulfate (mL), B: sample ferrosulfate (mL), N: normality, C: the amount of undiluted prototype (mg /L). Finally, the following formula was used to obtain the percentage of COD removal.

$$\text{COD removal \%} = \frac{C_0 - C}{C_0} \times 100$$

Here C<sub>0</sub> is the initial concentration of COD and C is the final concentration of COD [31]

### Checking seed effectiveness and analytical technique by using procedures in 5210B. 5-Day to make BOD measurement

In the first step, we considered 3 bottles (300 mL) with lids and measured the approximate concentration of BOD using COD. First, 2/3 of the bottle was filled with diluting water, and then the desired amount of sample was poured into it. After complete mixing, the bottles were filled completely with diluting water and sealed. They were placed in the incubator at 5 ° C for 5 days. 1 ml of MnSO<sub>4</sub> was added to the sample and after mixing 1 mL alkaline iodide (I) was introduced as well. In the presence of dissolved oxygen, the color of the solution turns into brown. When 2/3 of the floccants was settled, 1 mL of concentrated H<sub>2</sub>SO<sub>4</sub> was added on the surface of the sample and mixed until the floccants dissolved. 201 mL of the prepared sample was introduced into the Erlenmeyer flask and titrated with NaS<sub>2</sub>O<sub>3</sub> (0.025 M) until the color changed to yellow. A few drops of n(C<sub>6</sub>H<sub>10</sub>O<sub>5</sub>) glue was added, until the solution turned into blue. The solution was titrated again until white color appeared. The amount of dissolved oxygen in the sample is equal to the amount of titration used.

$$\text{BOD ((mg/l) O}_2) = \frac{(D_1 - D_2) - (S)V_s}{P}$$

$$P = \frac{S}{V}$$

Here are, D<sub>1</sub>: diluted oxygen of the diluted sample immediately after preparation (mg / L), D<sub>2</sub>: diluted oxygen of the diluted sample after 5 days of incubation at 20 ° C (mg / L), P: percentage

of sample added, V: Sample volume in sample test bottle (mL), S: sample volume added to bottle 300 (mL). Finally, the following formula was used to obtain the percentage of BOD removal.

$$\text{BOD removal \%} = \frac{C_0 - C}{C_0} \times 100$$

Here  $C_0$  is the initial concentration of BOD and  $C$  is the final concentration of BOD [31].

## Instruments

In order to characterize the intermediates and catalysts, the following instruments were employed: Philips CM30300Kv instrument (for recording Transmission electron microscopy (TEM) images), Siemens, model D5000 diffractometer using Cu- $K\alpha$  radiation as the X-ray source (for recording X-ray diffraction (XRD) patterns), PERKIN-ELMER-Spectrum 65 spectrometer, with KBr pellets (for conducting Fourier transform infrared (FT-IR) spectroscopy), the field emission scanning electron microscope (SIGMA VP model, ZEISS, Germany), and EDS and Mapping Detector Specifications (Oxford Instrument Company UK).

## Result and discussion

### Characterization of $\text{TiO}_2@WO_3/\text{ZnO}$ photocatalyst

To illustrate  $\text{TiO}_2@WO_3/\text{ZnO}$  photocatalyst, FT-IR spectrum of the as-prepared catalyst was recorded. As shown in Figure 1, the absorbance bands can be observed at  $3382\text{--}3525\text{ cm}^{-1}$  (-OH),  $2888\text{ cm}^{-1}$  (-CH<sub>2</sub>),  $1195\text{ cm}^{-1}$  (etheric CO). Moreover, the peaks in the fingerprint area at  $837$ ,  $663$ , and  $517\text{ cm}^{-1}$  corresponded to the  $\text{TiO}_2$ ,  $\text{WO}_3$ , and  $\text{ZnO}$  nanoparticles [40].

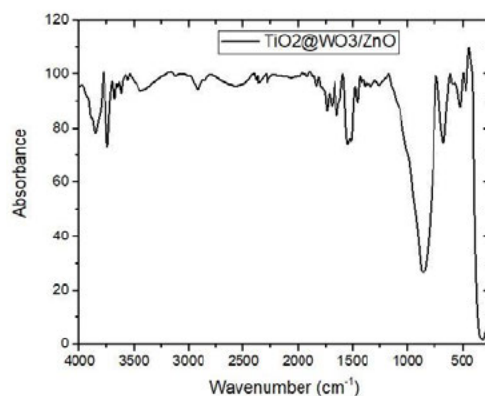


Figure 1. FT-IR spectrum of as-synthesized  $\text{TiO}_2@WO_3/\text{ZnO}$  photocatalyst.

The synthesized  $\text{TiO}_2@/\text{WO}_3/\text{ZnO}$  photocatalyst was analyzed by means of BET. In fact, this method by measuring the amount of  $\text{N}_2$  gas adsorbed and desorbed by the analyte surface identified the surface area of cavities at a constant temperature. By comparing the BET curve of  $\text{TiO}_2@/\text{WO}_3/\text{ZnO}$  photocatalyst with standard diagram (Figure 2a). Evidently, between relative pressures of 0.05 to 0.3 the plot was closely linear. Furthermore, according to the International Union of Pure and Applied Chemistry (IUPAC) classification,  $\text{N}_2$  adsorption–desorption isotherms of the synthesized photocatalyst were of type III isotherms with  $\text{H}_3$  hysteresis loops, Figure 2b and this photocatalyst belongs to the group of mesopore materials [41, 42]. Moreover, the BET surface area for  $\text{TiO}_2@/\text{WO}_3/\text{ZnO}$  photocatalyst was significant ( $11.56 \text{ m}^2 \text{ g}^{-1}$ ). The high surface area of photocatalyst was promising for the degradation of alkanolamine since it ensures sufficient adsorption of contaminant molecules on the active sites which enhances catalytic efficiency [29, 43].

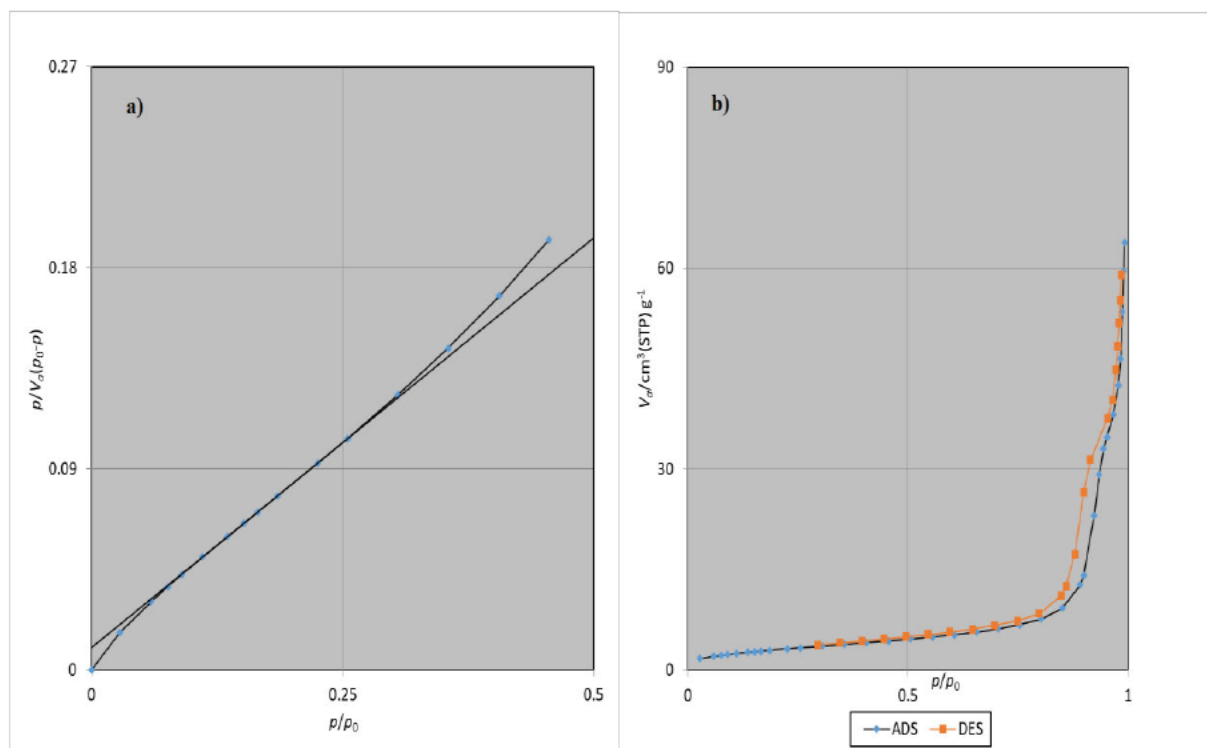


Figure 2. a) Standard diagram and b) adsorption-desorption isotherm of  $\text{TiO}_2@/\text{WO}_3/\text{ZnO}$  photocatalyst.

To get more information about the pore structure of the synthesized  $\text{TiO}_2@/\text{WO}_3/\text{ZnO}$  photocatalyst, the BJH method was employed, Figure 3. The results revealed that specific surface area, volume and diameter of the cavities were  $10.3 \text{ m}^2 \text{ g}^{-1}$ ,  $0.094 \text{ cm}^3 \text{ g}^{-1}$  and  $10.9 \text{ nm}$ , respectively. In fact, the pores diameter was mainly in the range of 6-30 nm, which further confirmed the existence of mesopores.

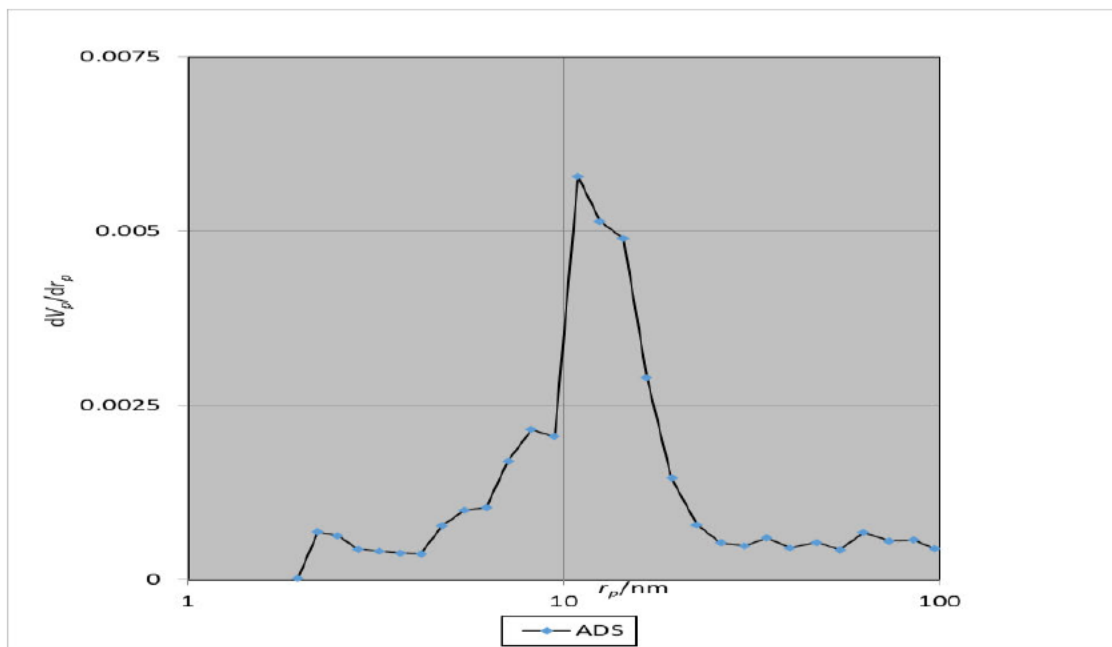


Figure 3. BJH pore size distribution of the synthesized  $\text{TiO}_2@/\text{WO}_3/\text{ZnO}$  photocatalyst.

In the following, it was studied whether  $\text{TiO}_2$  and  $\text{WO}_3/\text{ZnO}$  crystal structures were influenced in the catalyst synthesis step, Figure 4a. In the XRD pattern of  $\text{TiO}_2$ , some peaks observed at  $2\theta = 25.281, 37.801, 48.050, 53.891, 55.062$  and  $62.690^\circ$  which represent the tetragonal structure (JCPDS, NO. 021-1272, Figure 4b). Moreover, in the XRD pattern of  $\text{WO}_3/\text{ZnO}$  different peaks were detected at  $2\theta = 15.479, 18.907, 23.836, 24.572, 30.474, 30.721, 31.261, 36.313, 36.435, 38.337, 41.325, 44.233, 44.623, 45.450, 45.839, 48.763, 50.286, 51.721, 53.635, 54.264, 55.263, 56.156, 58.446, 61.767, 62.246, 65.054, 65.516$  and  $68.243^\circ$  which represent the monoclinic structure of the substance (JCPDS, No. 015-0774, Figure 4b). Finally, in the XRD pattern of the synthesized catalyst, nearly almost all peaks related to the  $\text{TiO}_2$  and  $\text{WO}_3/\text{ZnO}$  ingredients could be detected which confirmed the successful synthesis of the designed photocatalyst [44].

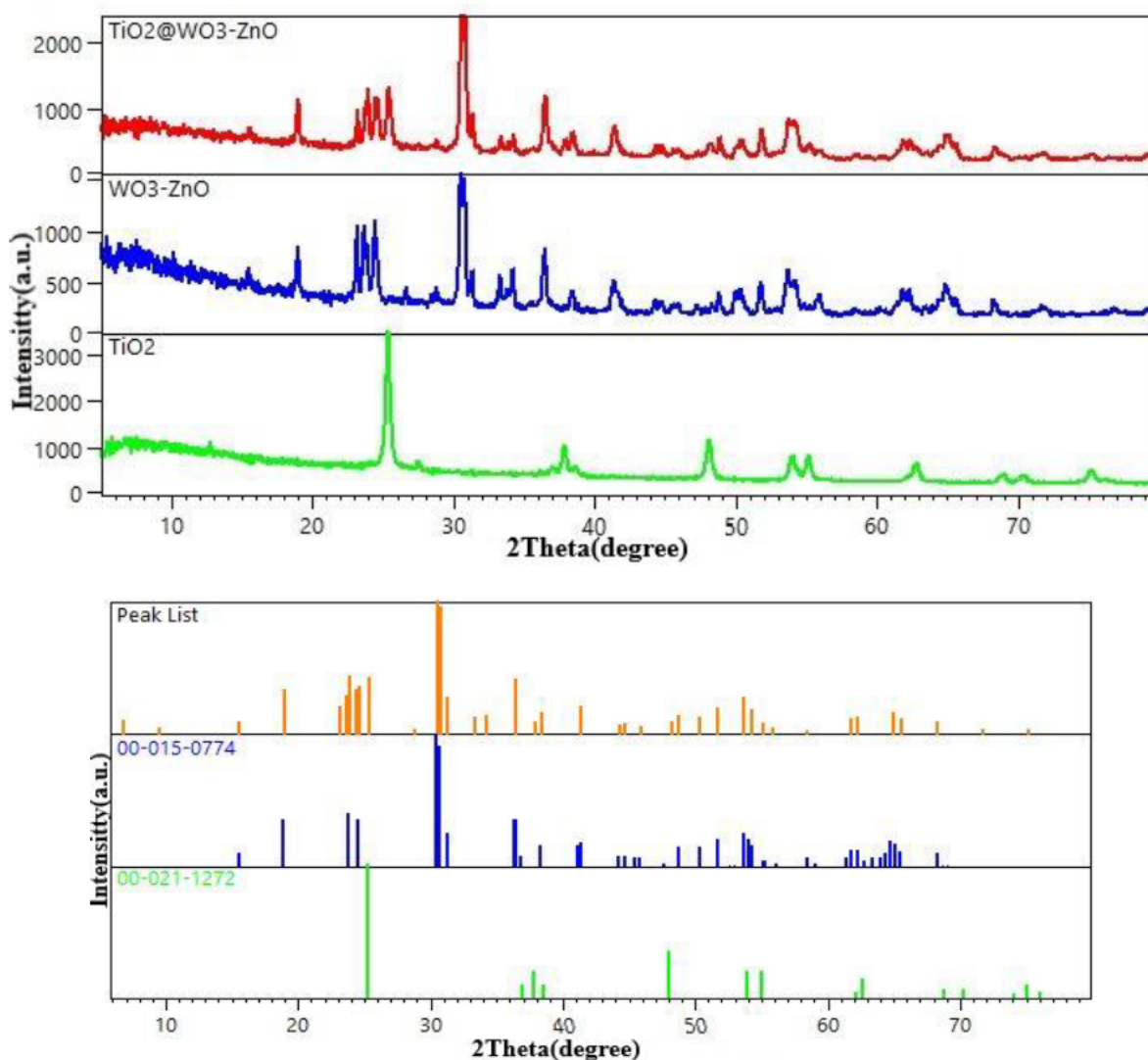


Figure 4. XRD pattern of WO<sub>3</sub>/ZnO, TiO<sub>2</sub>, and TiO<sub>2</sub>@WO<sub>3</sub>/ZnO photocatalyst nanoparticles.

FE-SEM images of as-synthesized WO<sub>3</sub>/ZnO and TiO<sub>2</sub>@WO<sub>3</sub>/ZnO were divulged in Figure 5. As illustrated, both samples demonstrate flake-like morphology. In the EDS curve of the WO<sub>3</sub>/ZnO (Figure 5a right), the elements of W, O and Zn can be detected. Characterization of TiO<sub>2</sub>@WO<sub>3</sub>/ZnO via EDS analysis, Figure 5b right, indicated the presence of Ti, O, W, and Zn atoms in the structure of the as-prepared photocatalyst. The elemental mapping analysis of W, O, Ti and Zn elements, Figure 6, revealed homogenous dispersion of studied elements which can enhance catalytic efficiency.

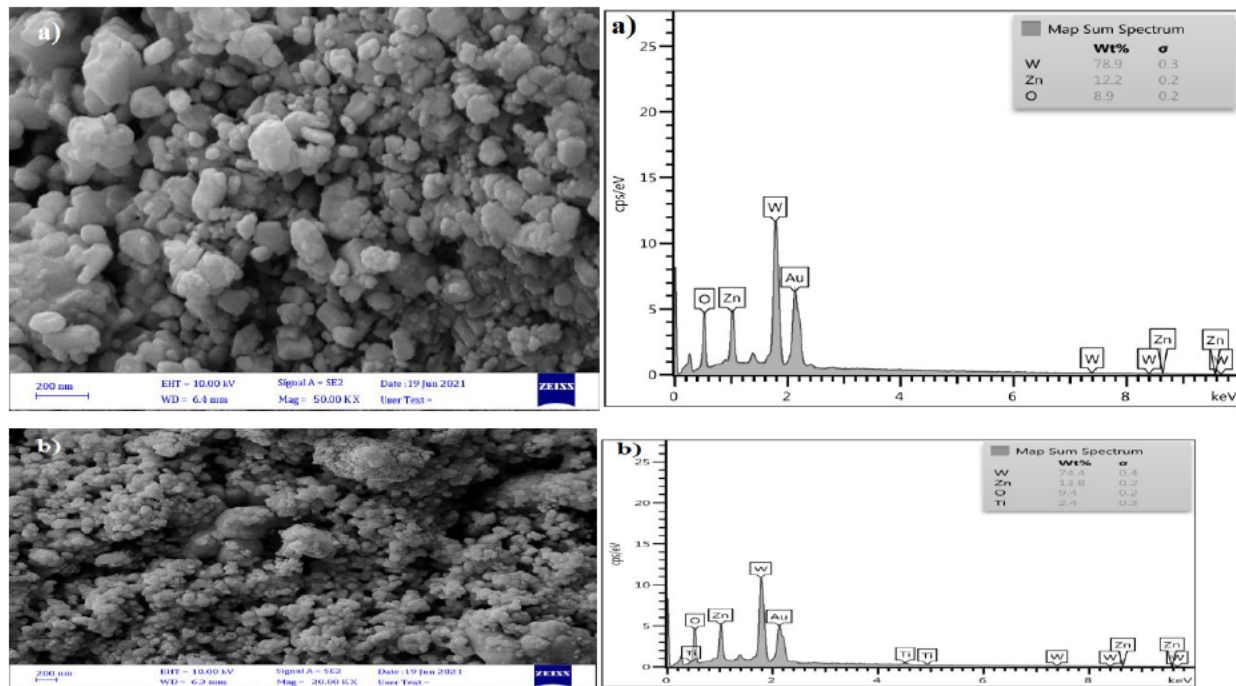


Figure 5. Left: FE-SEM images of: a) WO<sub>3</sub>/ZnO photocatalyst b) TiO<sub>2</sub>@WO<sub>3</sub>/ZnO photocatalyst and Right: EDS of: a) WO<sub>3</sub>/ZnO photocatalyst b) TiO<sub>2</sub>@WO<sub>3</sub>/ZnO photocatalyst.

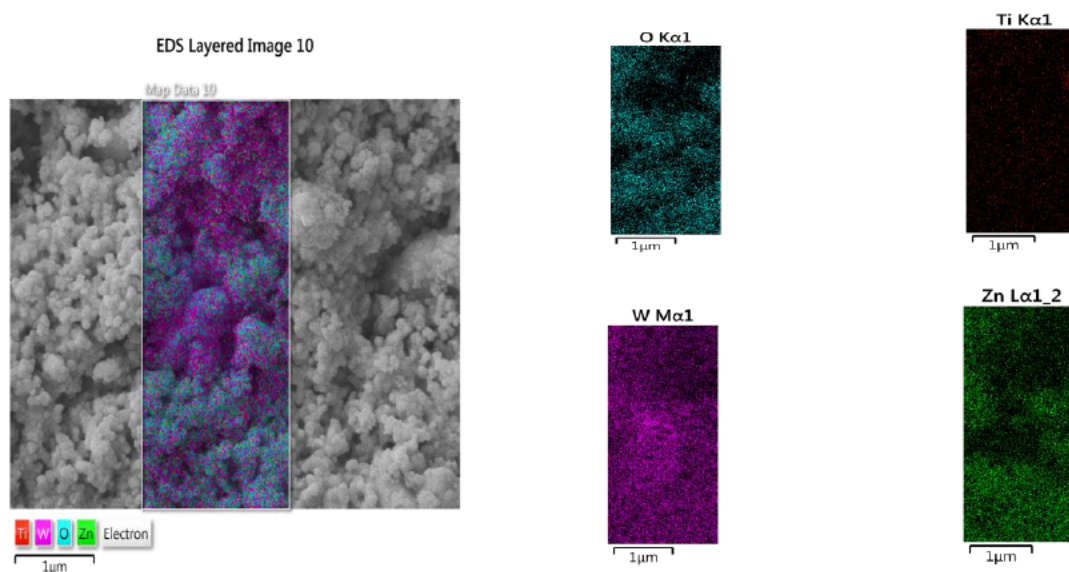


Figure 6. Representative mapping of O, Ti, W and Zn elements of TiO<sub>2</sub>@WO<sub>3</sub>/ZnO photocatalyst.

More detailed morphological information was achieved from the TEM pattern of synthesized  $\text{TiO}_2@/\text{WO}_3/\text{ZnO}$  photocatalyst, Figure 7. As illustrated, spherical and cubic morphologies of the catalyst particles with an average particle length of 900 nm and a width of 300 nm can be detected. In fact, it is observed that the aggregations of spherical and cubic structures that can be originated from the presence of ZnO and  $\text{TiO}_2$  nanoparticles as detected in FE-SEM and EDS.

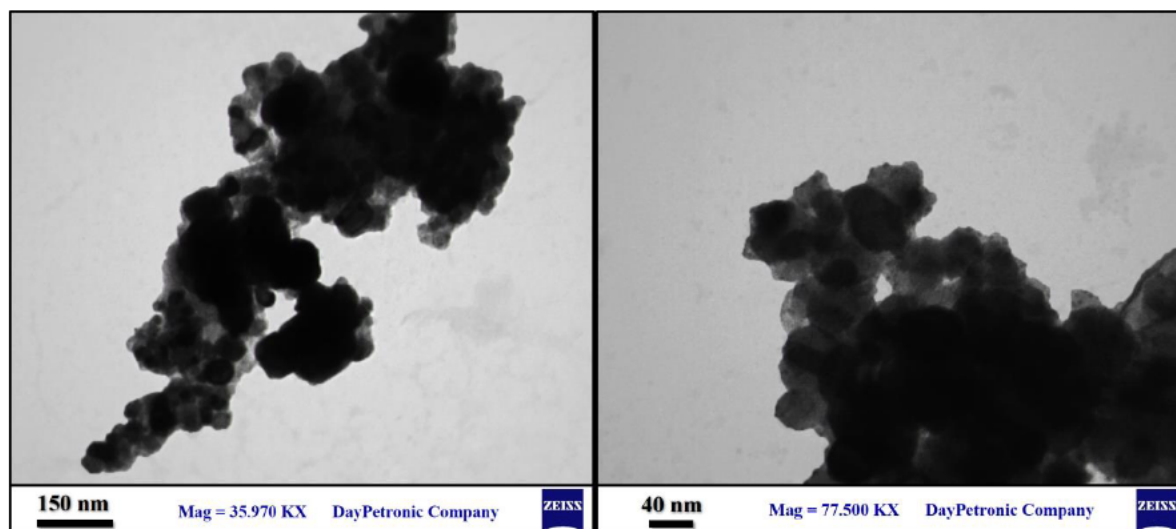


Figure 7. TEM image of  $\text{TiO}_2@/\text{WO}_3/\text{ZnO}$  photocatalyst at 40 and 150 nm scale.

### Photocatalyst optimization

In order to better rationalize the photocatalytic activity of the synthesized catalyst, it is crucial to analyze its band gap using a spectrophotometer. By the way, the method of penetration reflection spectroscopy was employed which relies on the reflection of light in the ultraviolet (11-421 nm), visible (421-711 nm) and infrared (711-2511 nm) areas. In this method, the achieved spectra were interpreted according to Kubelka-Monk theory as equation 1:

$$F(R_\infty) = \frac{(1-R_\infty)^2}{2R_\infty} = \frac{\alpha}{S} \quad (1)$$

In which, the expression  $F(R_\infty)$  was a function of Kubelka Monk,  $\alpha$  and  $S$  were the absorption coefficient and the scattering constant, respectively, and  $R_\infty$  was the diffusion reflection coefficient, that was calculated according to the equation 2.

$$R_\infty = \frac{R_{sample}}{R_{standard}} \quad (2)$$

where,  $R_{\text{sample}}$  and  $R_{\text{standard}}$  stand for the reflection coefficient of the sample and standard material, respectively. To get the tape distance, the Taoist rule (equation 3) was employed:

$$(\alpha h \nu)^{1/2} = A(h \nu - E_g) \quad (3)$$

In this formula,  $\alpha$ ,  $\nu$ ,  $E_g$  and  $A$  were the absorption coefficient, the frequency of the incident light, the band distance and the equation constant, respectively. Using equations 1-3, the Kubelka-Monk function was derived from the data of diffusion-reflectance spectrum according to formula 4.

$$[F(R)h \nu]^{1/2} = A(h \nu - E_g) \quad (4)$$

By plotting  $(F(R)h \nu)^{1/2}$  versus  $h\nu$ , the band gap ( $E_g$ ) was obtained from the extending of the linear section of the curve onto the horizontal axis. Lowering of  $E_g$  level by proper selection of the photocatalyst ingredients and optimizing their amounts are crucial factors in designing highly active photocatalysts. In this regard,  $\text{WO}_3/\text{ZnO}$  and  $\text{TiO}_2@\text{WO}_3/\text{ZnO}$  with different weight fractions were synthesized and their spectrophotometric property in terms of  $E_g$  value was analyzed. Figure 8 demonstrates the curves taken from the spectrophotometric analysis of the  $\text{TiO}_2$ ,  $\text{WO}_3$ ,  $\text{WO}_3/\text{ZnO}$  and  $\text{TiO}_2@\text{WO}_3/\text{ZnO}$  photocatalyst. As aforementioned previously, these energies were obtained from the extrapolation of the  $(\alpha h\nu)^{1/2} - h\nu$  curves to the  $(\alpha h\nu)^{1/2}=0$ . In the obtained spectra from spectrophotometer, the activity of the synthesized photocatalyst was indicated by advent of absorption edge in the visible light region. This was related to the energy gap via previously mentioned equations. Among  $\text{ZnO}$ ,  $\text{TiO}_2$  and  $\text{WO}_3$  the later exhibited the lowest bond gap energy of 2.8 eV (Figure 8a). In the  $\text{WO}_3/\text{ZnO}$  alloy with optimized weight ratio of 1:4,  $E_g$  decreased to 2.6 eV (Figure 8b). In the case of synthesized  $\text{TiO}_2@\text{WO}_3/\text{ZnO}$  photocatalyst with optimized  $\text{TiO}_2/\text{WO}_3+\text{ZnO}$  weight ratio of 1:3, the  $E_g$  reached its minimum value of 2.1 eV. The low  $E_g$  amount facilitates the mechanism of electron-hole generation and improves the photocatalytic activity/efficiency in visible light region [38, 39].

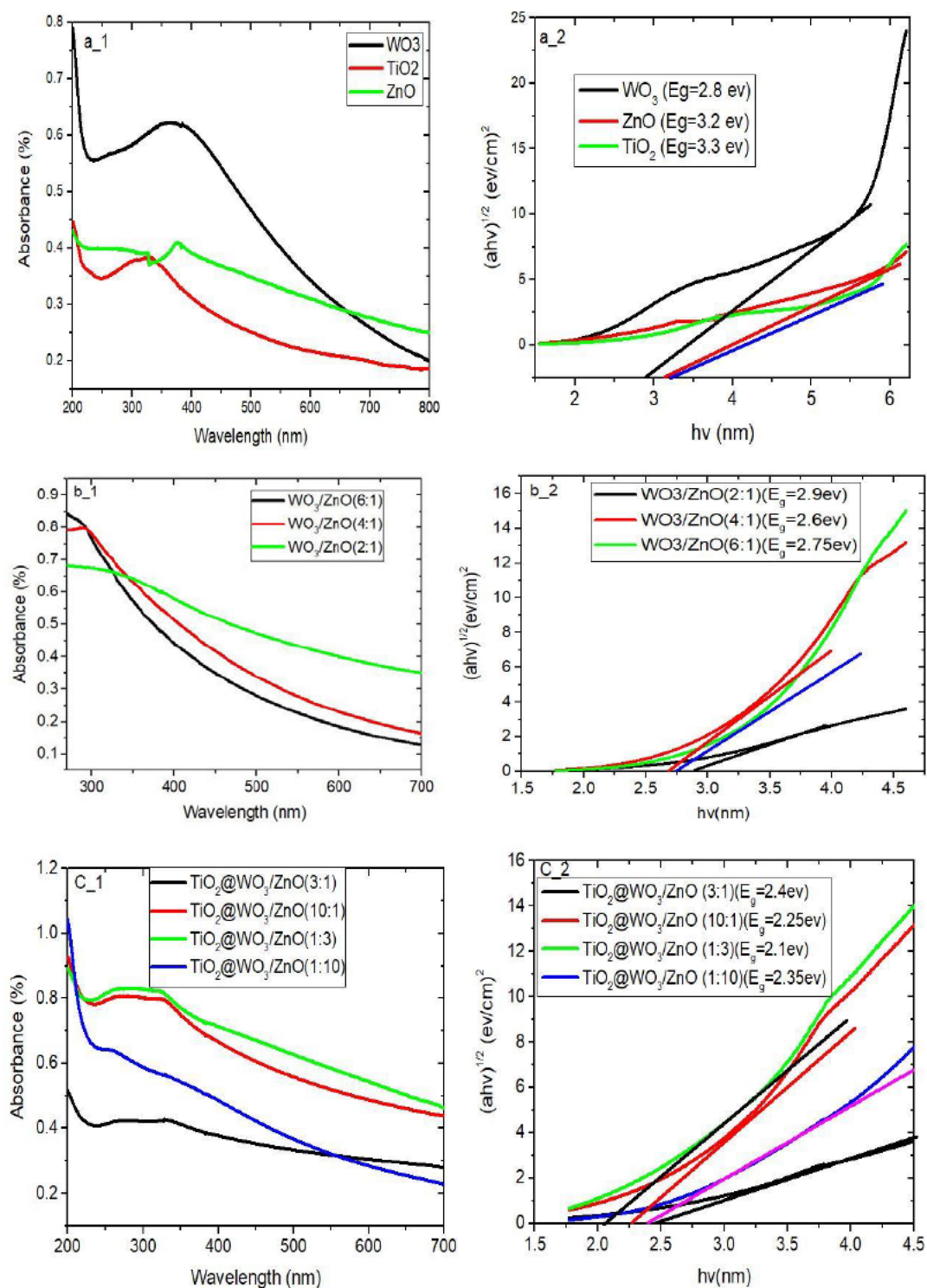


Figure 8. Left: spectrophotometric analysis and Right:  $(ah\nu)^{1/2}$  - $h\nu$  curves and  $E_g$  values of a)  $WO_3$ ,  $ZnO$  and  $TiO_2$  , b)  $WO_3/ZnO$  (with 6:1, 4:1 and 2:1 weight ratios) and c)  $TiO_2@WO_3/ZnO$  (with 3:1, 10:1, 1:3 and 1:10 weight ratios)

Along with the obtained results from this section,  $\text{TiO}_2@\text{WO}_3/\text{ZnO}$  with 3:1 weight ratio of  $\text{TiO}_2$  to  $\text{WO}_3+\text{ZnO}$  was selected as the catalyst of choice since it contained optimized ingredients weight fraction. In the following, photocatalytic activity of this catalyst was studied in detail.

### Photocatalytic activity and spectral characteristics

To evaluate the catalytic efficiency of the  $\text{TiO}_2@\text{WO}_3/\text{ZnO}$  photocatalyst, the oxidation reaction of alkanolamine contaminant from waste water of gas refinery effluent was performed in the presence of LED light and the progress of reaction was monitored using UV–visible spectroscopy. In this regard, the effect of the LED exposure time on the degradation of alkanolamine was evaluated (Figure 9). The decrease of the absorbance at  $\lambda_{\text{max}}=296\text{ nm}$  demonstrated efficient degradation of contaminants so that 68 % of the contaminants were decomposed in a short reaction time of only 40 min. It approved good efficiency of the synthesized  $\text{TiO}_2@\text{WO}_3/\text{ZnO}$  photocatalyst. Indeed, in the designed photocatalyst, with optimized structure, because of the effective charge separation and long lifetime of the electron–hole pairs generated in the photocatalyst, the gas refinery effluent photo-degradation by this heterojunction was efficient. In other words, the separated charge carriers could transfer to the surface of the photocatalyst and thus participate in the degradation reaction. This facilitated the photo-degradation of alkanolamine of waste water from gas refinery effluent.

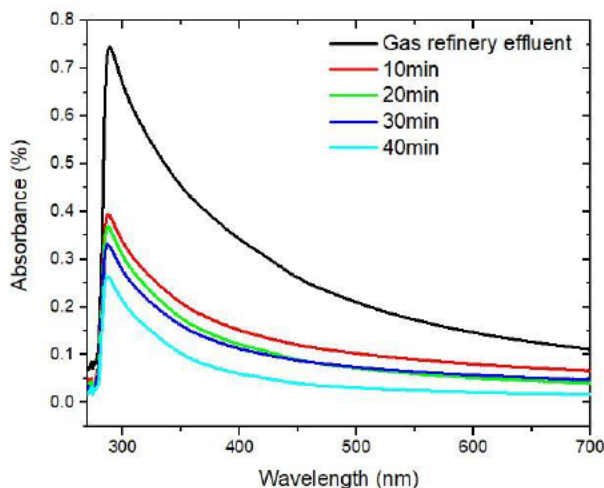


Figure 9. Time-dependent UV–Visible spectra for the catalytic degradation of alkanolamine of waste water from gas refinery effluent in the presence of LED light using as-synthesized  $\text{TiO}_2@\text{WO}_3/\text{ZnO}$  photocatalyst (catalyst dosage: 0.5 %).

## Fluorescence Spectra

Fluorescence emission and excitation spectra of alkanolamine of waste water from gas refinery effluent were illustrated in Figure 10. It was found that alkanolamine had intrinsic fluorescence in aqueous solution. Indeed, the maximum excitation wavelength of gas refinery effluent occurred at 285 nm, which corresponded to absorption peak of alkanolamine. Another peak was observed at 324 nm, correlated to the characteristic emission peak of alkanolamine. Therefore, the excitation and emission peaks were set at 285 and 324 nm, respectively. In the presence of  $\text{TiO}_2@WO_3/\text{ZnO}$  photocatalyst, the fluorescence intensity of alkanolamine decreased dramatically during 30 min LED light exposure, although, no substantial decrease in the the fluorescence intensity was detected during 10 min light exposure (Figure 10).

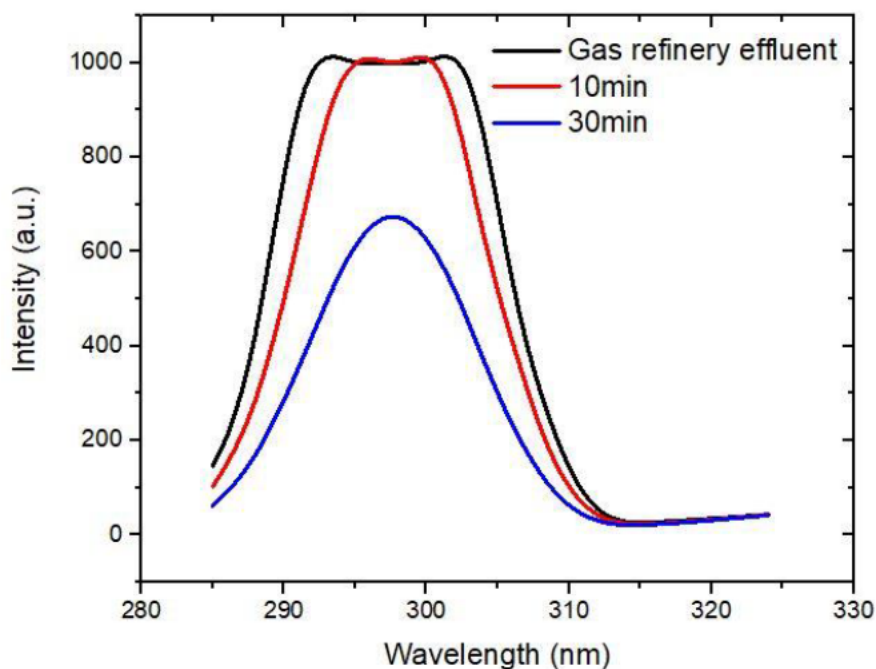


Figure 10. Fluorescence excitation and emission spectra of primary alkanolamine of waste water from a gas refinery effluent and it in the presence of the synthesized  $\text{TiO}_2@WO_3/\text{ZnO}$  photocatalyst after 10 and 30 min exposure to LED light (catalyst dosage: 0.5 %).

## Effect of LED irradiation time on COD and BOD removal

The composition (COD and BOD) of typical gas refinery effluent is shown in Table 1. Concentrated gas refinery effluent wastewater represents cases with low water consumption

whereas dilute wastewater represents high water consumption. Figure 11 shows the effect of LED irradiation time on the removal of organic compounds from the gas refinery effluent. LED irradiation time varied between 10 and 40 minutes. According to the laboratory results, the percentage of COD and BOD removal increased through enhancing LED irradiation time. It was as expected that radiation time has a great effect on the removal of organic compounds.

Table 1. COD and BOD parameters in gas refinery effluent.

Time (mine)	COD (mg/L)	BOD (mg/L)
0	125	72
10	68.75	37.44
20	62.75	33.12
30	47.5	28.08
40	41.25	20.1

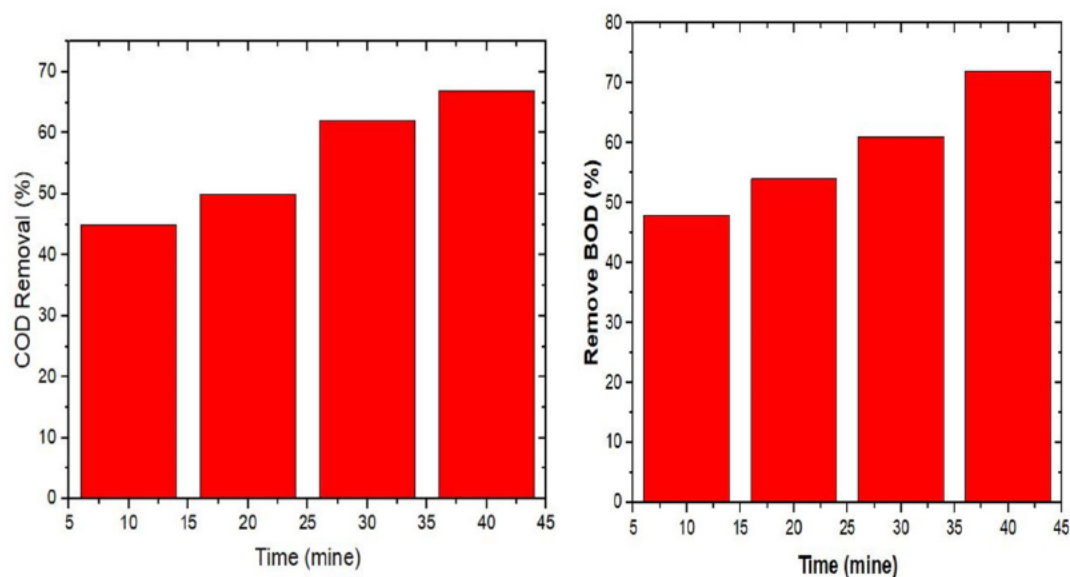
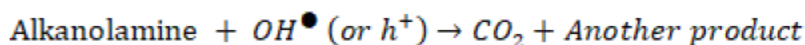
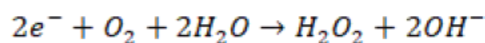
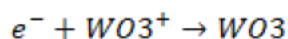
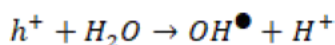
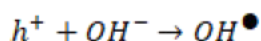
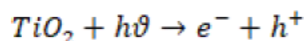


Figure 11. Effect of time on COD and BOD removal percentage (photocatalyst mass 0.15 g, effluent volume 30 mL, pH = 8.5)

### The mechanism of photocatalytic reaction

The suggested mechanism for the degradation of alkanolamine contaminant in the presence of  $\text{TiO}_2@/\text{WO}_3/\text{ZnO}$  photocatalyst was featured out in (Figure 12). In the as-synthesized photocatalyst, since the  $\text{TiO}_2$  (3.3 eV) band gap was larger than the  $\text{ZnO}$  (3.2 eV) and  $\text{WO}_3$  (2.8 eV), it had higher performance [45]. Since,  $\text{ZnO}$ ,  $\text{WO}_3$ , and  $\text{TiO}_2$  were in contact, electrons migrated from  $\text{WO}_3$  to  $\text{ZnO}$  and finally to the  $\text{TiO}_2$  conduction band to balance their Fermi surface. Thus at the  $\text{TiO}_2$  level electrons accumulated while  $\text{WO}_3$  had an additional positive charge. When the photocatalyst was exposed to visible light, electrons were transferred from the  $\text{TiO}_2$  capacitance band to the conduction band, simultaneously creating a hole in the number of  $\text{TiO}_2$  capacitance band electrons. As a result, excited electrons could be rapidly transferred from  $\text{TiO}_2$  to  $\text{ZnO}$  and eventually to  $\text{WO}_3$ , which reduced the composition of the electron hole [40]. Electrons collected on the surface of  $\text{TiO}_2$  conduction band may be transferred to the surface, where the oxygen absorbed on the surface was reduced to  $\text{H}_2\text{O}_2$  by the electrons. Correspondingly, pores due to visible radiation absorption, as a result of their high oxidation potential [46], could react with surface-bound  $\text{H}_2\text{O}$  or  $\bullet\text{OH}$  and hydroxyl  $\bullet\text{OH}$  free radicals. On the other hand, free radicals as a strong oxidizer, hydroxyl could react with organic pollutants to make them safer compounds. The photocatalytic reactions performed are as the follows.



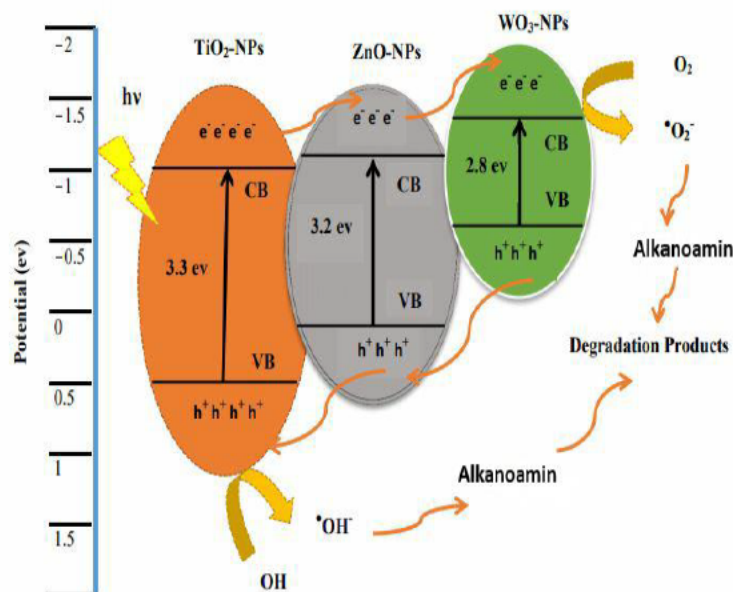


Figure 12. Suggested mechanism for the photocatalytic degradation of alkanolamine contaminant over the  $\text{TiO}_2@/\text{WO}_3/\text{ZnO}$  photocatalysts.

## Conclusions

By the proper selection of  $\text{TiO}_2$  to  $\text{WO}_3+\text{ZnO}$  and  $\text{WO}_3$  to  $\text{ZnO}$  weight ratios a new heterogenous photocatalyst,  $\text{TiO}_2@/\text{WO}_3/\text{ZnO}$ , was furnished. The resulting photocatalyst was characterized and applied in the degradation of alkanolamine contaminant to treat waste water from an industrial gas refinery complex. The outcomes indicated that the desined catalyst in the optimized weight ratio of ingredienct had remarkable efficiency. In this respect,  $\text{TiO}_2$  nanoparticles after adding to  $\text{WO}_3/\text{ZnO}$  to furnish  $\text{TiO}_2@/\text{WO}_3/\text{ZnO}$ , increased the photocatalytic activity by reducing the band gap of the photocatalyst (from 2.6 to 2.1 eV). The designed photocatalyst presented a very good efficiency of 68 % in the decomposition of alkanolamine of waste water after exposure to LED light for 40 min using very low catalyst loading of only 0.5 wt. %. Holistically, this catalyst is an environmentally friendly sample that can be easily precipitated for the sake of its heterogenous nature.

## Author Contributions

Paymaneh Taghizadeh-Lendeh did all experiments and analyses. Amir Hossein Mohsen Sarrafi and Afshar Alihosseini helped in conceptualization, Methodology and editing the manuscript. Naeimeh Bahri-Laleh has role in Methodology and writing and editing of the manuscript.

## References

- [1] S. Shoji, X. Peng, A. Yamaguchi, R. Watanabe, C. Fukuhara, Y. Cho, T. Yamamoto, S. Matsumura, M-W. Yu, S. Ishii, T. Fujita, H. Abe, M. Miyauchi, *Nat Catal.*, 3, 14153 (2020)
- [2] S. Harimurti, A.A. Omar, A.U. Rahmah, T. Murugesan, *IEEE.*, (2011)
- [3] A. Ali Hosseini, H. Seyyed Hossein, *Energy exploration & exploitation.*, 30, 389 (2012)
- [4] C.S. Lu, C.C. Chen, F.D. Mai, H.K. Li, *J Hazard Mater.*, 165, 306 (2009)
- [5] N. Riaz, M.A. Bustam, F.K. Chong, Z.B. Man, M.S. Khan, A.M. Shariff, *Sci. World J.*, 342020 (2014)
- [6] M. Muscetta, L. Clarizia, C. Garlisi, G. Palmisano, R. Marotta, R. Andreozzi, *Di Somma I, Int J Hydrog Energy.*, 45, 26701 (2020)
- [7]. R.M. Ramli, C.F. Kait, A.A. Omar, *Procedia Eng.*, 148, 508 (2016)
- [8] S.C. Jung, I.S. Park, H.J. Bang, Y.K. Park, S.J. Kim, K.J. Jeon, K.H. Chung, *Chem Eng J.*, 386, 121552 (2020)
- [9] Ghaedi, M., *Photocatalysis: Fundamental Processes and Applications*, Elsevier, (2021)
- [10] A. Taghizadeh, M. Taghizadeh, M. M. Sabzehmeidani, F. Sadeghfar, M. Ghaedi, *Interface Sci. Technol.*, 32, 1 (2021)
- [11] F. Sadeghfar, Z. Zalipour, M. Taghizadeh, A. Taghizadeh, M. Ghaedi, *Interface Sci. Technol.*, 32, 55 (2021)
- [12] H. Tahir, M. Saad, *Interface Sci. Technol.*, 32, 125 (2021)
- [13] F. Sadeghfar, M. Ghaedi, Z. Zalipour, *Interface Sci. Technol.*, 32, 225 (2021)
- [14] F. Sadeghfar, S. Bahrani, M. Ghaedi, *Interface Sci. Technol.*, 32, 375 (2021)
- [15] S. Bahrani, M. Ghaedi, R. Tariq, Z. Zalipour, F. Sadeghfar, *Interface Sci. Technol.*, 32, 499 (2021)
- [16] Z. Moradi, S.Z. Jahromi, M. Ghaedi, *Interface Sci. Technol.*, 32, 557 (2021)
- [17] S. Mosleh, M.R. Rahimi, M. Ghaedi, *Interface Sci. Technol.*, 32, 673 (2021)

- [18] F. Sadeghfar, M. Ghaedi, *Interface Sci. Technol.*, 32, 725 (2021)
- [19] U.A. Fegade, G.N. Jethave, *Interface Sci. Technol.*, 32, 871 (2021)
- [20] P. Wadhera, R. Jindal, R. Dogra, *Iran Polym J.*, 29, 501 (2020)
- [21] K.H. Chung, Y.K. Park, E.B. Cho, B.J. Kim, S.C. Jung, *Int J Hydrog Energy.*, 45, 24028 (2020)
- [22] V. S. Bhamare, R. M. Kulkarni, A. A. Parwaz Khan, Elsevier. 171 (2021)
- [23] M.K. Yazdi, V. Vatanpour, A. Taghizadeh, M. Taghizadeh, M.R. Ganjali, M.T. Munir, S. Habibzadeh, M.R. Saeb, M. Ghaedi, *Mater Sci Eng C.*, 114, 111023 (2020)
- [24] A. H. Saeedi Dehaghani, V. Pirouzfard, A. Alihosseini, *Polym. Bull.*, 12(77) :6467 (2020)
- [25] M. Parthibavarman, M. Karthik, S. Prabhakaran, *Vacuum.*, 155, 224 (2018)
- [26] Y.L. Ying, S. Y. Pung, S. Sreekantan, Y. F. Yee, M. T. Ong, Y. F. Pung, *Mater Today: Proc.*, 17, 1008 (2019)
- [27] B. Nam, T.K. Ko, S. Hyun, C. Lee, *Appl Surf Sci.*, 504, 144104 (2020)
- [28] J. Sun, L. Sun, N. Han, J. Pan, W. Liu, S. Bai, Y. Feng, R. Luo, D. Li, A. Chen, *Sens Actuators B Chem.*, 285, 68 (2019)
- [29] R.A. AbuMousa, U. Baig, M.A. Gondal, M. A. Dastageer, M. S. AlSalhi, B. Mofteh, F. Yahya Alqahtani, S. Akhter, F. Sfouq Aleanizy, *Saudi J Biol Sci.*, 27, 1743 (2020)
- [30] Y. M. Hunge, A. A. Yadav, V. L. Mathe, *Ultrason Sonochem.*, 45, 11122 (2018)
- [31] W. Chen, H. Shen, X. Zhu, H. Yao, W. Wang, *Ceram. Int.*, 41, 14008 (2015)
- [32] R. B. Baird, A. D. Eaton, E. W. Rice, *American Public Health Association.*, (2017)
- [33] S. Karimi, S. Sadjadi, N. Bahri-Laleh, M. Nekoomanesh-Haghighi, *Mol Catal.*, 509, 111648 (2021)
- [34] S. Karimi, N. Bahri-Laleh, G. Pareras, S. Sadjadi, M. Nekoomanesh-Haghighi, A. Poater, *J Ind Eng Chem.*, 97, 441 (2021)
- [35] C. Pragathiswaran, C. Smitha, H. Barabadi, M. M. Al-Ansari, L. A. Al-Humaid, M. Saravanan, *Inorg Chem Commun.*, 121, 108210 (2020)
- [36] M. K. Otoufi, M. Ranjbar, A. Kermanpur, N. Taghavinia, M. Minbashi, M. Forouzandeh, F. Ebadi, *Solar Energy*, 208, 697 (2020)
- [37] H.I.S. Nogueira, A.M.V. Cavaleiro, J. Rocha, T. Trindade, J.D.P. de Jesus, *Mater Res Bull.*, 39, 683 (2004)

- [38] M.H. Barzegar, M. Ghaedi, V. Madadi Avargani, M.M. Sabzehmeidani, F. Sadeghfar, R. Jannesar, *Polyhedron.*, 165, 1 (2019)
- [39] M.H. Barzegar, M. Ghaedi, V. Madadi Avargani, M.M. Sabzehmeidani, F. Sadeghfar, R. Jannesar, *Polyhedron.*, 158, 506 (2019)
- [40] R. Abe, H. Takami, N. Murakami, B. Ohtani, *J Am Chem Soc.*, 130, 7780 (2008)
- [41] M. Tabrizi, S. Sadjadi, G. Pareras, M. Nekoomanesh-Haghighi, N. Bahri-Laleh, A. Poater, *J Colloid Interface Sci.*, 581: 939 (2021)
- [42] X. Han, B. Yao, K. Li, W. Zhu, X. Zhang, *J Chem.*, 2390486 (2020)
- [43] R.W. Coughlin, F.S. Ezra, *Environ Sci Technol.*, 2, 291 (1968)
- [44] H. Qin, L. Chen, X. Yu, M. Wu, Z. Yan, *J Mater Sci: Mater Electron.*, (2018), <https://doi.org/10.1007/s10854-017-8119-4>
- [45] G. Vida, V.K. Josepovits, M. Győr, P. Deák, *Microsc. Microanal.*, 9: 337 (2003)
- [46] T. Arai, M. Yanagida, Y. Konishi, Y. Iwasaki, H. Sugihara, K. Sayama, *J Phys Chem C.*, 111, 7574 (2007)

#### HOW TO CITE THIS ARTICLE

Paymaneh Taghizadeh-Lendeh, Amir Hossein Mohsen Sarrafi, Afshar Alihosseini, Naeimeh Bahri-Laleh, “**Investigating the photocatalytic activity of TiO<sub>2</sub>@WO<sub>3</sub>/ZnO catalyst in the waste water treatment containing alkanolamine contaminants**” *International Journal of New Chemistry.*,2022, DOI: 10.22034/ijnc.2022.4.2.